Structural characterization of a putative recombinant L-amino acid oxidase from *Leptospira interrogans*

D. Vaigundan[1], I. Yuvaraj[2,†], P. Sunita[3], K. Sekar[2], M. R. N. Murthy[3,5] and P. R. Krishnaswamy[1,4,*]

[1]Genomics and Central Research Laboratory, Department of Cell Biology and Molecular Genetics, Sri Devaraj Urs Academy of Higher Education and Research, Tamaka, Kolar 563 101, India
[2]Computational Data Sciences, [3]Molecular Biophysics Unit, and
[4]Centre for Nanoscience and Engineering, Indian Institute of Science, Bengaluru 560 012, India
[5]Institute of Bioinformatics and Applied Biotechnology, Bengaluru 560 100, India
[†]Present address: National Institute for Plant Biotechnology, Indian Council of Agricultural Research, New Delhi 110 012, India

Amino acid oxidases (AOs) are flavin adenine dinucleotide (FAD)-dependent dimeric enzymes that stereo specifically catalyse the deamination of an α-amino acid leading to an α-keto acid. Putative *Leptospira interrogans* recombinant L-amino acid oxidase (*Li*-rLAO; lacking 20 residues corresponding to the N-terminal signal sequence) was cloned, expressed, purified, and its three-dimensional structure was determined by X-ray crystallography at a resolution of 1.8 Å. The active site could be easily identified by the presence of electron density corresponding to a non-covalently bound FAD in both protomers of the dimeric enzyme. Structural analysis of *Li*-rLAO revealed that its polypeptide fold is similar to those of the previously determined homologous structures as available in the Protein Data Bank. However, a substrate-binding residue found at the active site of other previously determined homologous structures was not conserved in *Li*-rLAO, suggesting that its specificity may differ from those of earlier reported structures. Not surprisingly, *Li*-rLAO showed no activity for most amino acids and amines; it exhibited a low activity only with L-arginine as the substrate. The catalytic properties of *Li*-rLAO could be rationalized in terms of its three-dimensional structure.

Keywords: Amino acid oxidase, dimeric enzyme, homologous structures, *Leptospira interrogans*, structural analysis.

LEPTOSPIRES are obligate, aerobic, motile, tightly coiled, spiral-shaped bacteria measuring 0.1 μm in diameter and 6–20 μm in length[1–6]. Weil observed a condition leading to severe jaundice in people dwelling in marshy areas. In 1914, Inada and Ido identified and confirmed that *Leptospira* was the causative agent leading to severe jaundice (leptospirosis)[1]. Kidney is the main target of *Leptospira* sp. Ultrastructural study of mice kidney after infecting with *Leptospira* sp. demonstrated that the species enters by penetration of the capillary lumen, followed by entry into the interstitial tissue causing oedema and cellular infiltration at days 4–8. *Leptospira* sp. is found in the proximal tubular cells on day 10 of infection[7–9]. Acute kidney injury resulting from tubulointerstitial nephritis is an early and primary manifestation of systemic leptospirosis[10]. The proximal tubule of the kidney is a rich source of amino acids. In most mammals, ~99% of filtered amino acids are reabsorbed in the proximal tubule, which allows utilization of ~70 g amino acids/day in a 70 kg person. The excretion of most amino acids is limited to between 0.2% and 2.5%, although this may increase in various pathologic conditions[11–17]. *Leptospira* finds a haven here, evading the immune system and utilizing the rich nitrogenous source for survival. Therefore, enzymes that help utilize amino acids in *Leptospira* sp. are likely to be suitable targets for the design of drugs against the pathogen.

L-amino acid oxidase (LAO; EC 1.4.3.2) activity was studied for the first time by Zeller[18] in 1944. In the human kidney, there is an LAO and a D-amino acid oxidase that stereo specifically catalyses the oxidative deamination of almost all L- and D-amino acids. In the kidney, D-amino acid oxidase activity is higher than that of LAO, which is important for detoxifying D-amino acids derived from bacteria and a few other sources[19,20]. Phylogenetically, LAO from animals are clustered with gastropod enzymes. Biochemical and structural studies have been conducted on LAOs of snake venom (svLAOs), fishes and mammals[21,22]. svLAOs have been the subject of many studies, and several reviews have been published dealing with their biochemical properties and their importance in pharmacology[23–25]. svLAOs are usually homodimeric glycoproteins with subunit molecular weights of around 50–70 kDa and use non-covalently linked FAD (flavin adenine dinucleotide) or FMN (flavin mononucleotide) as the cofactor for catalysis[24,26]. In contrast to svLAO, very little is known about LAOs from microorganisms. In recent years, many bacterial enzymes have been shown to exhibit LAO activity[20,25]. The bacterial

*For correspondence. (e-mail: p.r.krishnaswamy@gmail.com)

enzymes do not cluster into well-defined groups[25]. The enzymatic properties of LAOs from microbial sources are usually distinct in terms of the optimum pH for catalysis, substrate specificity and stability[20,27–29].

The availability of the complete genome sequence for both pathogenic and non-pathogenic *Leptospira* provides an opportunity to explore this organism's metabolic enzymes systematically. Proteomic analysis has provided evidence for a secreted putative L-amino acid oxidase (NCBI ref. sequence: WP_000778112.1 &NZ_LMAQ010000327.1; Uniprot ID: IQ65_19870; UniProtKB entry: A0A098MN43) in cultures of *Leptospira*[30]. There is no report in the literature on the biochemical characterization of this putative LAO. This 447-residue polypeptide sequence contains an *N*-terminal putative signal peptide referred to as the TAT (twin-arginine translocation) signal sequence[31], which may be cleaved after membrane transport. The present study reports the structural and biophysical characterization of the putative *Leptospira interrogans* recombinant L-amino acid oxidase (*Li*-rLAO), lacking 20 residues corresponding to the *N*-terminal signal sequence.

Materials

Escherichia coli strains Top10, DH5α, BL21 (DE3) and C41 were a generous gift from A. Pennmatsa (MBU, IISc), pET21b plasmid was a generous gift from M. Vijayan (MBU, IISc). The 6× DNA loading dye, dNTPs, protein markers and DNA ladder were procured from Bangalore Genei, India. PHUSION DNA polymerase, pre-stained marker (Thermo Scientific, USA), *NdeI*, *Xho1*, *Dpn1* endonucleases were from NEB. Plasmid isolation kit (Qiagen, Germany), Tris, BSA, FAD, dialysis membrane, ethidium bromide, DTT, agarose, sodium dodecyl sulphate and PMSF were purchased from Sigma, USA. Primers were procured from Eurofins, India; sodium chloride, EDTA, glycerol, acrylamide, bis-acrylamide, bromophenol blue, ammonium persulphate, TEMED, glycine were from SDFCL; amino acid substrates L-histidine, L-alanine, L-tryptophan, L-methionine L-glutamine, L-asparagine, L-glutamate, L-aspartate, L-serine, L-arginine, L-proline and L-tyrosine were from Sigma (a generous gift from P. Balaram (MBU, IISc) and J. Chatterjee (MBU, IISc)); L-phenylalanine, L-leucine, L-isoleucine, L-valine and L-threonine were obtained from Sisco Research Laboratories Pvt Ltd. Amine substrates Dopamine and Spermine (Sigma, USA) were also gifted by A. Pennmatsa (MBU, IISc). Spermidine (Sigma, USA) was a gift from B. Gopal (MBU, IISc); Histamine HCl was from HiMedia, Putrescine, and Tryptamine (Sigma, USA) from P. Balaram.

Methods

Sequence analysis of putative leptospiral LAO

BLASTP and PSI blast[32] were used to find sequences in the SWISS-PROT database homologous to *Li*-rLAO. The motifs present in the sequence of *Li*-rLAO were located using the motif search protocol in Pfam[33] and conserved domain database[34]. Multiple sequence alignment with homologs was achieved using the UniProt Knowledge database (UniProt. 2017) and UniProt Align[35].

Cloning

The polynucleotide corresponding to *Li*-rLAO (without the N-terminal 20-amino acid signal peptide) obtained from the pET21b plasmid containing the full-length *Li*-LAO gene cloned between *Nde1* and *XhoI* sites was amplified by site-directed mutagenesis using Phusion polymerase with the forward primer: ATGGGCCTTCCAGGAATAAAATTAAGTG and the reverse primer: ATGTATATCTCCTTCTTAAAGTTAAAC, under the following conditions: initial denaturation at 95°C for 30 sec, followed by 16 cycles consisting of the following steps: denaturation at 95°C for 30 sec, annealing at 55°C for 1 min, PCR amplification at 68°C for 7 min followed by a final extension step at 68°C for 5 min. The amplified PCR product was treated with *Dpn1* for one hour and directly transformed into DH5α cells. The clone was confirmed by DNA sequencing.

The pET21b plasmid containing the *Li*-rLAO gene was transformed into *E. coli* strain C41 and grown in Luria Bertani broth (LB) for 8–10 h with 100 μg/ml ampicillin. The culture was used as a 1% pre-inoculum in LB culture grown at 37°C. After induction with 500 μM IPTG (when $OD_{600\ nm}$ was ~0.6–0.8), the culture was allowed to grow for another 16 h at 30°C. Cells were harvested by centrifugation (20 min, 5440 *g*, 4°C), resuspended in lysis buffer containing 20 mM Tris-HCl (pH 6.8), 1 mM EDTA, 1 mM PMSF, 1 mM DTT, and 10% glycerol (lysis buffer to bacterial culture volume was in the ratio 1 : 20) and disrupted by sonication (35% amplitude, 20 sec off and 10 sec on, 25 cycles). After centrifugation (45 min, 22,900 *g*, 4°C) and removal of cell debris, the supernatant was subjected to SP sepharose cation exchange chromatography (0.5 ml/min). The column was pre-equilibrated with 20 mM Tris-HCl (pH 6.8) with a flow rate of 1 ml/min and washed with 20 mM Tris-HCl (pH 6.8). The bound protein was eluted with a linear gradient containing 100 ml of buffer A (20 mM Tris-HCl pH 6.8) and 100 ml of buffer B (20 mM Tris-HCl pH 6.8 with 1 M sodium chloride) with a flow rate of 1 ml/min. Fractions of 10 ml were collected using a fraction collector.

The pooled fractions were concentrated using a 30 kDa cut-off Amicon® Ultra-15 Centrifugal Filter Unit (1060 *g*, 4°C). The concentrated protein was subjected to gel filtration chromatography (HiLoad 16/600 Superdex 200 pg column, Amersham Biosciences, USA), pre-equilibrated with 20 mM Tris-HCl (pH 6.8) containing 100 mM sodium chloride (ÄKTA Basic 10 HPLC system, GE Healthcare). The purity of the protein obtained by gel filtration was checked on SDS-PAGE. LC-ESI/MS was used to determine the accurate mass of the protein. The concentration of purified protein was estimated by the Bradford method.

Mass spectrometry

Electrospray ionization mass spectra were recorded on maXis impact Q-TOF (Bruker Daltonics, Bremen, Germany) coupled to Agilent 1200 series online HPLC. The spectrometer was tuned using a standard Agilent ESI Tune mix ranging from 118 to 2721 *m*/*z* in the positive-ion mode. Data processing was done using the deconvolution module of the Data Analysis 4.1 software (Bruker Daltonics, Bremen, Germany) to identify multiple charge states of the protein and obtain the derived mass.

In-gel trypsin digestion and MS/MS

The bands corresponding to *Li*-rLAO protein were cut out from Coomassie brilliant blue-stained 10% SDS-PAGE (reducing) gel and subjected to tryptic digestion using sequencing grade modified trypsin (Promega Corporation)[36]. In brief, stained gel pieces were excised, minced into 1 mm^3 size, and transferred to a sterile centrifuge tube. The gel pieces were washed with 500 µl of wash buffer (50% acetonitrile, 50 mM ammonium bicarbonate) till the Coomassie dye was removed. Destained gel pieces were dehydrated in 100% acetonitrile for 5 min and rehydrated in 150 µl reduction solution (10 mM DTT, 100 mM ammonium bicarbonate) for 30 min at 56°C. The sample obtained was incubated with 100 µl of alkylating solution (50 mM iodoacetamide, 100 mM ammonium bicarbonate) for 30 min in the dark at room temperature. Reduced and alkylated gel pieces were washed with wash solution, dehydrated with 100% acetonitrile for 5 min and completely dried at room temperature in a centrifugal evaporator. Gel pieces were rehydrated with 20 µl of sequencing-grade trypsin (20 µg/ml) and incubated overnight at 37°C. The digested peptides were extracted from the gel pieces with an extraction solution (50% acetonitrile, 0.1% TFA). The extracted peptides from each sample were further concentrated in a vacuum concentrator and subjected to MS/MS analysis.

Analytical gel filtration

Analytical gel filtration chromatography was performed on a Superdex 200 increase 10/300 GL (GE Healthcare) column to determine the oligomeric state of the purified protein. Gel filtration was done on a pre-equilibrated column at a flow rate of 0.2 ml/min, using 20 mM Tris-HCl buffer (pH 6.8) containing 100 mM NaCl. The protein solution was centrifuged at 22,900 *g* for 20 min at 4°C, and the clear supernatant was injected into the column. The injection volume was 500 µl with a protein concentration of ~140 µM. Absorbances at 220 and 280 nm were recorded to monitor the elution of the protein. Molecular weight standards, carbonic anhydrase (19 kDa), alcohol dehydrogenase (150 kDa), albumin (66 kDa), apo-ferritin (443 kDa), beta-amylase (200 kDa) and thyroglobulin (669 kDa) were used to calibrate the column pre-equilibrated with 50 mM tris-HCl buffer (pH 7.2) containing 100 mM KCl with a flow rate of 0.2 ml/min.

Circular dichroism spectrum and thermal denaturation

The circular dichroism (CD) spectrum was recorded on a JASCO-715 spectropolarimeter (JASCO technologies, Tokyo, Japan) equipped with a thermostat cell-holder controlled by a Peltier device using a 2 nm bandpass and a cuvette of 1 mm path length. The purified protein (~90 µM in 20 mM tris-HCl, pH 6.8) was maintained at different temperatures (25°–65°C at 5°C temperature intervals) for thermal melting studies. Three CD scans were recorded at a scan speed of 10 nm min^{-1} at each temperature. The HT voltage remained in the permissible range throughout the scans.

Spectroscopic characterization

The fluorescence spectra of the purified protein were recorded on an F2500 fluorescence spectrophotometer (Hitachi Science and Technology, Japan) using a protein concentration of ~285 µM, with excitation wavelengths of 450 and 280 nm. Spectra were recorded in the range 480–800 nm and 300–800 nm respectively.

Crystallization

The purified protein was concentrated to ~20 mg/ml, centrifuged at 22,900 *g* for 1 h at 4°C and screened for crystallization conditions using Hampton crystal screen kits by the under-oil method. Crystals were obtained in the 95th condition of the index screen in a crystallization drop containing 1 µl of (~20 mg/ml) protein and 1 µl of crystallization condition (HR2-944-95 containing 0.1 M potassium thiocyanate, 30% w/v polyethylene glycol monomethyl ether 2000) at 298 K. Initially the crystals were small in size due to excessive nucleation. To overcome this, the condition was diluted with 1 µl of water before mixing with the protein solution. Good quality crystals appeared in about two weeks.

Data collection, structure solution and refinement

A native crystal was mounted on a cryo-loop and flash-frozen in liquid nitrogen. X-ray diffraction data were collected on the Beamline XRD1/XRD2 at Elettra Synchrotron Trieste, Italy, with the oscillation angle set to 0.5°. The native crystal diffracted to 1.78 Å resolution. Data were processed with iMOSFLM and XIA2-DIALS of the CCP4i2 suite of programs[37–42]. The intensity data obtained were used for structure determination by molecular replacement using Phaser, MrBUMP, MolREP and the automated

Table 1. Diffraction data and refinement statistics of putative *Leptospira interrogans* recombinant L-amino acid oxidase (*Li*-rLAO)

Parameters	*Li*-rLAO (KI-soaked)	*Li*-rLAO (native)
Wavelength (Å)	1.5498	1.07
Resolution limits (Å)	69.68–1.95 (1.95–1.95)	84.61–1.78 (1.81–1.78)
Unit cell dimensions (Å)	51.776, 105.915, 139.363 ($\alpha = \beta = \gamma = 90$)	51.75, 106.22, 139.91 ($\alpha = \beta = \gamma = 90$)
Space group	P 2_1 2_1 2_1	P 2_1 2_1 2_1
*R*merge (%)	14.1 (15.9)	11.8 (39.0)
No. of unique reflections	44,824	74,369
No. of molecules in the asymmetric unit	2	2
Completeness (%)	78.6 (11.7)	99.1 (99.8)
Multiplicity	22.1 (3.2)	11.3 (12.1)
Mean ((I) > $\alpha(I)$)	16.2 (0.6)	14.3 (5.9)
*R*work/*R*free (%)	–	17.7/22.3
RMSD bond length (Å)	–	0.0147
RMSD bond angle (°)	–	1.834
Average *B*-factors (Å2)		
Protein	–	17.18
Water	–	25.08
Ligands	–	9.14
Ramachandran statistics (%)		
Favoured region	–	94.2
Allowed region	–	5.55
Outliers	–	0.25

The values in parenthesis correspond to the highest resolution range.

structure determination server AUTORICKSHAW[43,44], utilizing svLAO(PDB id: 2IID, 3KVE, 1REO) as the phasing model. However, none of the molecular replacement programs provided an acceptable solution. Further, the data were also examined in MarathonMR, which uses various domains available in the domain database as models for structure determination[45]. Even these efforts were unsuccessful.

In order to obtain a solution for the crystal structure using a possible signal from a suitable anomalous scatterer, crystals were soaked in a crystallization cocktail containing 0.5 M potassium iodide (1 M of potassium iodide mixed with the crystallization condition in a 1 : 1 ratio) for 15 min, mounted on a cryo-loop, flash-frozen in liquid nitrogen and X-ray diffraction data were collected on the Beamline XRD1/XRD2 at Elettra Synchrotron, Trieste. Data were collected twice for the same crystal with 0.5° oscillation; both the data were merged after renaming the files. The merged data were processed with iMOSFLM and XIA2-DIALS of the CCP4i2 suite of programs[37–42]. The crystal soaked with KI diffracted to 2.38 Å resolution. Iodine sites in the crystal were located using the anomalous signal, and the substructure of iodine atoms was determined by Crank 2.0 of the CCP4i2 package[46–53]. The program SHELX identified nine iodine atoms. An initial model with 829 residues (R = 0.27; Rfree = 0.35) was built using Crank 2.0. Manual model building and refinement of the structure were carried out using Coot[54] v0.7.2.1 and REFMAC (version 5.5.0109)[55–60] respectively. The refined model was used as a template for molecular replacement with a native data set[61,62], which had diffracted up to 1.78 Å. Further, manual model building and refinement were carried out to obtain the final model with an *R*-factor of 0.18 and *R*free of 0.22. The asymmetric unit was compatible with two protomers and 39% solvent content. The data between 84.64 and 1.78 Å were included throughout the refinement calculations. Five per cent of the data was randomly chosen for free *R*-factor calculation. Table 1 shows the data collection, processing statistics and refinement parameters. The *Li*-rLAO coordinate file has been deposited in the Protein Data Bank (PDB ID: 7EME).

Structural analysis

Solvent-accessible area and interface residue analysis, accessible and buried surface areas and ΔG for dimer dissociation were calculated using the PISA server[63–65]. Structures similar to *Li*-rLAO were identified using DALI[66–69], and the top hits were quantitatively compared to the structure of *Li*-rLAO using the SSM superpose option of Coot[54]. Ramachandran map for the structures was generated using Procheck and Rampage. All molecular illustrations were prepared using Pymol, version 1.2r1.

Amino acid oxidase assay

The assay was conducted in a 96-well microplate in duplicates, following the procedure described by Kishimoto and

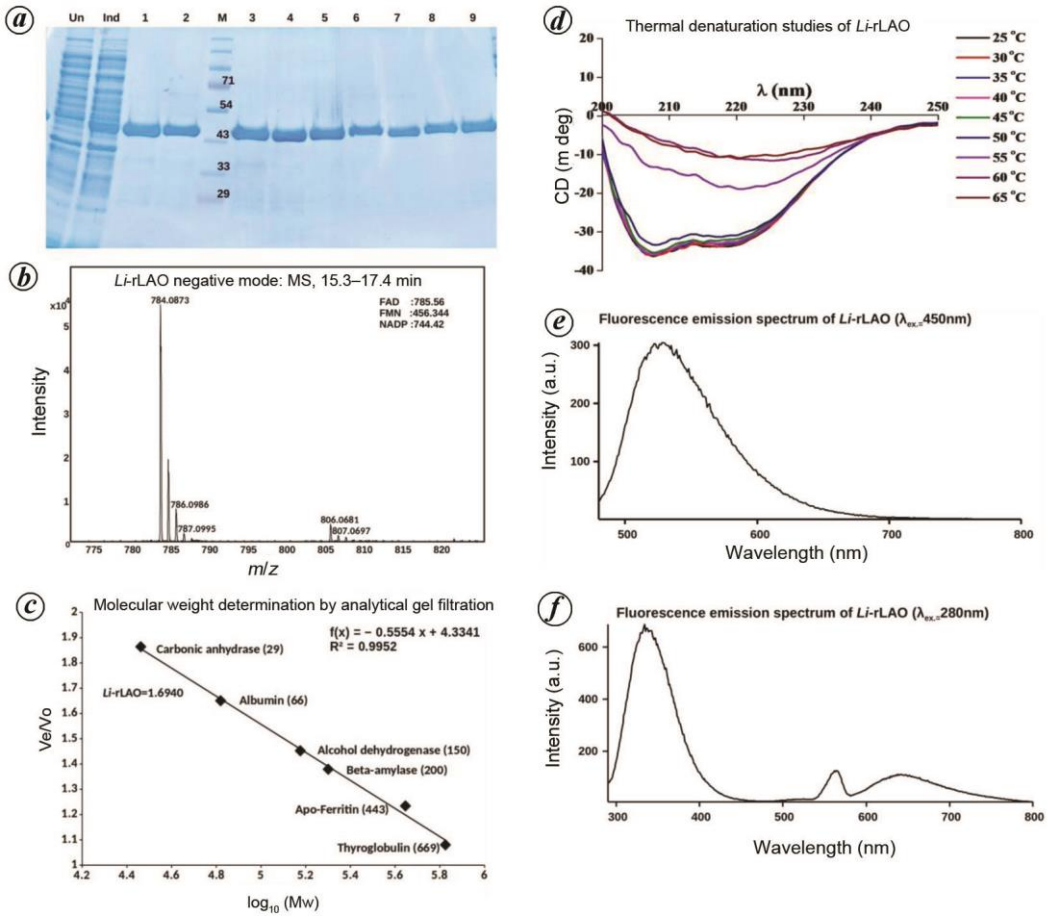

Figure 1. Purification and biophysical characterization of *Leptospira interrogans* recombinant L-amino acid oxidase (*Li*-rLAO). ***a***, Representative SDS-PAGE showing expression and purification of *Li*-rLAO. Lanes Un, Ind and M represent uninduced, induced and protein molecular weight markers respectively. The purified *Li*-rLAO fractions after gel filtration (HiLoad 16/600 Superdex 200 pg) chromatography are labelled 1–9. ***b***, Mass of flavin adenine dinucleotide (FAD) observed in purified *Li*-rLAO protein in the negative mode. ***c***, Standard graph obtained from analytical gel filtration column (Superdex 200 increase 10/300 GL) chromatography using molecular weight markers. ***d***, CD spectrum and thermal melting as monitored by recording CD spectra of *Li*-rLAO at different temperatures. ***e***, ***f***, Fluorescence emission spectra of *Li*-rLAO when excited at (***e***) 450 nm and (***f***) 280 nm.

Takahashi[70]. The standard reaction mixture contained L-amino acid substrate (initially 5 or 10 mM, at later stages, reduced to 2.5 mM), *Li*-rLAO (various concentrations ranging from 10 to 30 μM), 2 mM ortho-phenylene diamine (OPD), 0.81 U/ml horseradish peroxidase (HRP) and 50 mM borax–HCl buffer (pH 8.5) in a total volume of 100 μl/well. After incubation at 30°C for 45 min, the absorbance of the reaction mixture was measured by a microplate reader at 420, 492 and 630 nm. Further, the assay was also carried out in a phased manner, with amino acid substrates incubated with *Li*-rLAO (10–30 μM) for 45 min at 30°C followed by the addition of HRP and OPD and incubation at 30°C for another 45 min, making measurements after 90 min. The assay was carried out with all natural L-amino acids, except for L-cysteine and L-lysine.

Amine oxidase assay

The assay was conducted in a 96-well microplate in duplicate following the procedure described by Holt and Palcic with modifications[71]. The reaction was carried out in a mixture containing 50 mM HEPES, 5 mM KCl, 2 mM $CaCl_2$, 1.4 mM $MgCl_2$, 140 mM NaCl pH 7.4, 200 μM substrate, 500 μM 4-aminoantipyrene, 1 mM vanillic acid, 4 U ml^{-1} horseradish peroxidase and various concentrations of *Li*-rLAO (10–30 μM) for 30 min at 37°C. The absorbance of the reaction mixture was measured using a microplate reader at 498 nm. Putrescine, histamine, spermine, spermidine, dopamine and tryptamine were used as substrates in the assay.

Results

Sequence analysis

BLAST results suggested low amino acid sequence identities between *Li*-rLAO and other oxidases from various sources. The sequence alignment of LAOs from various organisms using PSI-BLAST indicated that *Li*-LAO aligned well with FAD-dependent oxidoreductases from bacteria.

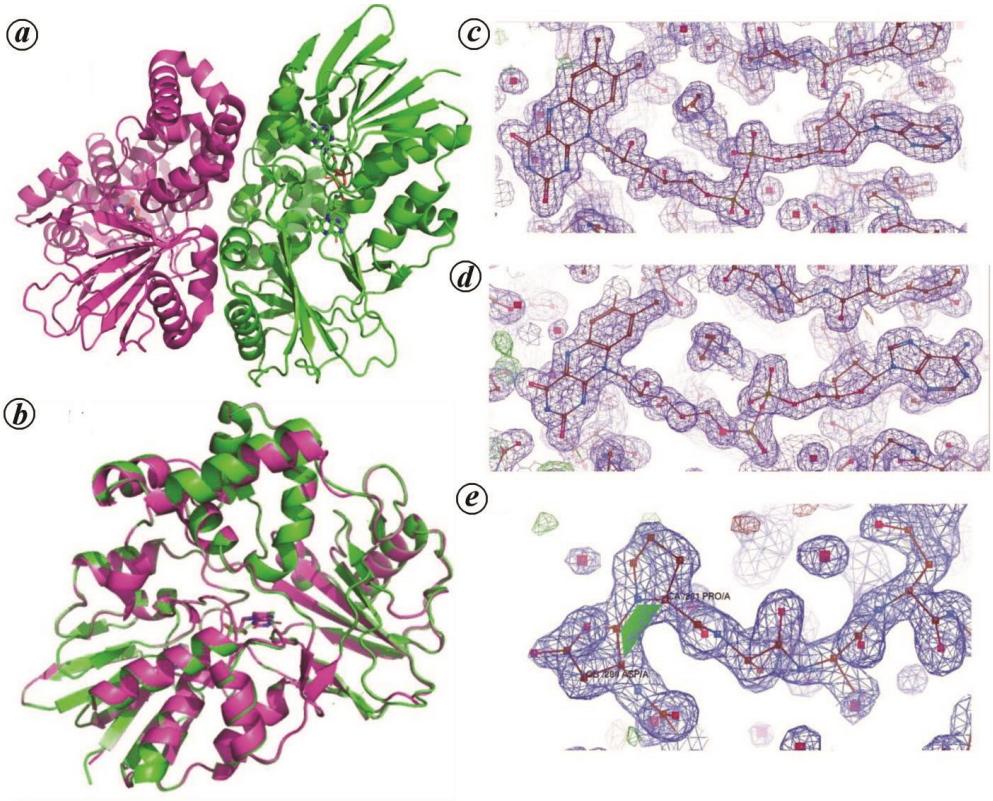

Figure 2. Structure of *Li*-rLAO. ***a***, Dimeric structure with subunit A represented in green and subunit B represented in pink colour. ***b***, Structural superposition of two subunits *Li*-rLAO illustrating the close similarity of their polypeptide folds. ***c***, 2Fo–Fc electron density corresponding to FAD bound to chain A of *Li*-rLAO. ***d***, 2Fo–Fc map of FAD bound to chain B of *Li*-rLAO. ***e***, Cis-peptide at Asp280 and Pro281 in the polypeptide fold of *Li*-rLAO.

Further, a search against Pfam and Conserved Domain Database (CDD) suggested that *Li*-rLAO may belong to the amino oxidase superfamily (data not shown).

Biochemical characterization

The *Li*-rLAO protein was purified from the lysate of *E. coli* C41 strain by SP-sepharose column followed by S200-Gel filtration chromatography. The yellow-coloured protein was easily collected from the protein-bound SP-sepharose column. Protein purification was monitored by 280 nm absorption of fractions obtained by gel filtration chromatography. The fractions with significant absorption were checked for purity on 10% SDS-PAGE and pooled (Figure 1 *a*). The molecular mass of the purified protein was obtained from Q-TOF mass spectrometry. The protein showed a mass of 47,090 Da, which is 131 Da less than the calculated mass based on sequence, indicating that the N-terminal methionine was probably removed in the *E. coli* strain used (Supplementary Figure 1). Also, unlike mammalian enzymes, the protein is unlikely to be glycosylated. The protein was also subjected to mass spectrometry in the negative-ion mode, and the presence of FAD in the purified protein was confirmed by the molecular weight obtained (Figure 1 *b*). Further, the oligomeric state of the purified protein was established as a monomer by analytical gel filtration column chromatography (Figure 1 *c*). The identity of the purified protein was further confirmed by tryptic digestion followed by Q-TOF mass spectrometry and data analysis using the Mascot software (data not shown).

The CD spectrum suggested that the protein was well-folded. Thermal melting studies showed that the protein was stable till 50°C. At 55°C, it showed sharp melting (Figure 1 *d*). In the fluorescence spectrum of *Li*-rLAO, the bound FAD showed an absorption band at 450 nm (data not shown) and a broad fluorescence emission band with λ_{max} = 525 nm (Figure 1 *e*). The internal tryptophan fluorescence studies of purified protein showed a broad fluorescence emission band with λ_{max} = 330 nm when excited at 280 nm and two more peaks at 560 nm (probably corresponding to 280∗2 = 560 nm) and a peak at 640 nm (probably corresponding to a FAD radical; Figure 1 *f*)[72]. Further studies are needed to confirm the identity of these peaks.

Structural features

The X-ray diffraction (XRD) data on a *Li*-rLAO crystal were obtained using beamline XRD1/XRD2 at the Elettra Synchrotron Trieste. Structure determination and refinement followed standard crystallographic protocols (Table 1).

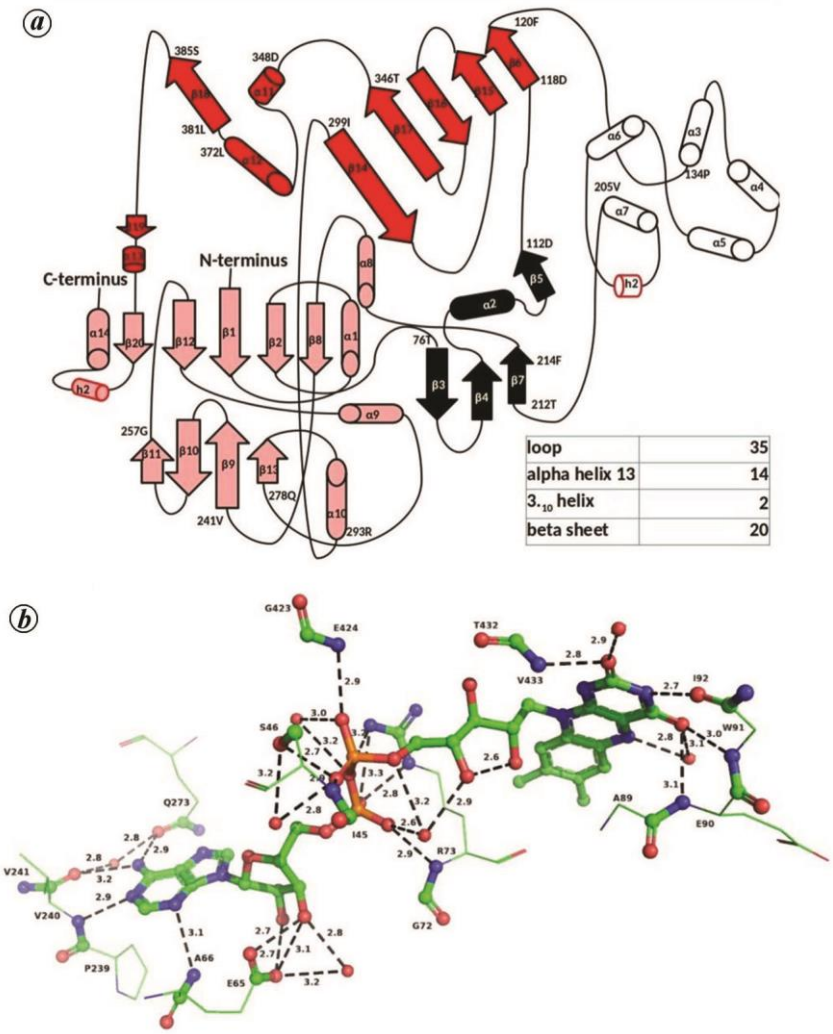

Figure 3. Structural organization of *Li*-rLAO. ***a***, Topological representation showing various domains. ***b***, Residues interacting with FAD in *Li*-rLAO.

Analytical gel filtration suggested that *Li*-rLAO exists as a monomer. However, the structure of the recombinant protein in the crystal suggested that it could assume a dimeric form as there were two protomers (A subunit (represented in green colour) and B subunit (represented in pink colour)) in the crystallographic asymmetric unit related by an approximate two-fold symmetry (Figure 2 *a*). The molecules packed as AB[FAD]$_2$ dimers with a protomer surface area of 30,850 Å^2 and a surface area buried in the dimeric interface of 6470 Å^2. The large interface area between subunits A and B suggested that the protein may assume a dimeric form under high concentrations. The superposition of the two subunits showed a root mean square deviation of 0.36 Å (Figure 2 *b*), suggesting no significant differences in the conformation of the two protomers. Both subunits showed electron density corresponding to a single, bound FAD molecule (Figure 2 *c* and *d*). Each subunit had a single *cis* peptide between Asp280 and Pro281 (Figure 2 *e*). Except for some N-terminal residues in both the chains and side chains of a few exposed residues, all main-chain atoms had well-defined electron densities. Examination of the Ramachandran plot illustrated that 92% of the residues were in the favoured region and 7.9% in the allowed region. The electron density was missing for the initial 14 residues of the A chain and 15 residues of the B chain. In chain A, electron density was missing for side chains of residues Ser34, Arg35, Lys36, Arg97, Lys109, Lys126, Glu138, Lys142, Lys209, Glu230, Asn231, Glu233, Lys249, Lys258, Lys259, Thr275, Gln374, Thr276 and Gln379, and in chain B for side chains of residues Lys36, Lys126, Glu138, Glu230, Glu247, Glu337, Gln374, Arg376, Glu377, Met416, Glu428, Arg428 and Val447.

The *Li*-rLAO protomer consisted of 15 α-helices, 19 β-sheets, and 33 loop regions (Figure 3 *a*). It contained a FAD-binding domain (β1–β2, β8–β13, β19, α1, α8–α10 or light pink), a C-terminal β-sheet domain (β6, β14–β18, α11 and α12 or red) with an α-helix sandwiched by five antiparallel β-sheets on one side, a single β-sheet on the other, and a helical domain with six α-helices (α2–α7 or white). All the domains were linked by the middle domain

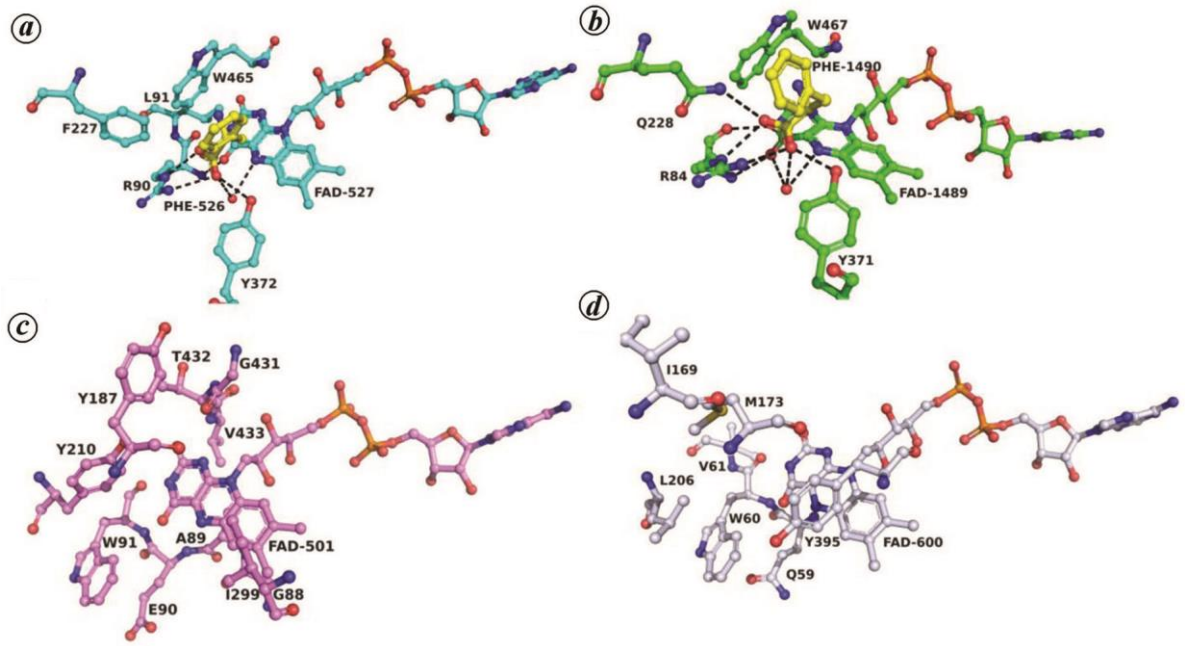

Figure 4. Structural comparison of LAOs. ***a*** and ***b***, Active-site residues with the bound amino acid substrate (yellow) in *Calloselasma rhodostoma* (PDB id: 2IID) and *Rhodococcus opacus* (PDB id: 2JB2) LAO respectively. (Hydrogen bonding between the arginine residue at the active site and the bound amino acid substrate (Phe) could be observed.) ***c***, Active site of leptospiral LAO. ***d***, Active site of *Rhodococcus erythropolis* putrescine oxidase (PDB id: 2YG3).

(β3–β5, β7 and α2 or black). Structural superposition using Coot[60] of *Li*-rLAO and other oxidases from various sources revealed the highest sequence identity (24.9%) with LAO from *Rhodococcus opacus* and the lowest (19.6%) with cyclohexylamine oxidase from *Brevibacterium oxydans*. Despite these low sequence identities, the overall three-dimensional structural fold of these proteins was remarkably similar, with the highest similarity from rat monoamine oxidase A (2.14 Å RMSD) and the lowest similarity from *Calloselasma rhodostoma* LAO (2.7 Å RMSD). Thus, these oxidases constitute a set of proteins with low amino acid sequence identity but high structural similarity. This observation is consistent with the diversity of substrates on which these oxidases are functional.

Li-rLAO contains the well-studied FAD-binding fold with a four-stranded, parallel β-sheet (β1–β2–β8–β12) sandwiched between a three-stranded, antiparallel β-sheet (β9–β10–β11) and an α-helix (α1). Strong hydrogen-bond networks hold FAD. The N1 atom of the adenine moiety of FAD forms a hydrogen bond with the backbone –NH atom of Val240. The N3 atom of adenine moiety of FAD forms a hydrogen bond with the backbone –NH atom of Ala66. The carboxyl group of Glu65 forms hydrogen bonds with –OH groups of ribofuranose ring (Figure 3 *b*). The N6 atom of adenine forms a hydrogen bond with the backbone –C=O of Val240 and sidechain amide (–C=O) of Gln273. The phosphate moiety attached to the ribofuranose forms a hydrogen bond with a conserved Arg73 side chain and its backbone –NH. The phosphate attached to the ribityl moiety forms hydrogen bonds with the backbone –NH of Ser46 and its side chain –OH group. This serine is also present in putrescine oxidase, but is substituted by threonine in most flavin-dependent oxidoreductases. Further, a backbone –NH of Glu424 also forms a hydrogen bond with the phosphate moiety. The ribityl moiety forms an internal hydrogen bond with hydroxyl groups at C2′ and C4′ positions, and with a conserved water molecule surrounding it. The peptide stretch Leu87–Ala89 is at a distance of about 4 Å from the isoalloxazine ring. It may form a barrier to the entry of molecules from the bulk solvent towards FAD. The isoalloxazine ring of FAD is held by hydrogen bonding only with the backbone atoms of the protein chain. The N1 atom of the isoalloxazine ring is not involved in hydrogen bonds. Carbonyl group at C2 forms a hydrogen bond with the backbone –NH of Val433 and two water molecules. One of these water molecules forms a hydrogen bond with His96. The N3 atom forms a hydrogen bond with the backbone –C=O of Trp91. The N5 atom of the isoalloxazine ring forms a hydrogen bond with a water molecule, which in turn is involved in a hydrogen bond network with Lys301 and Glu90. However, these interactions are not conserved in all other FAD-dependent oxidases. The guanidino group of Arg interacting with the phosphate of FAD and the side chain carboxyl group of a Glu interacting with the hydroxyl group of ribofuranose are common features of all structures. Similarly, the adenine moieties N1 and N6 interacting with a Pro and Val are also observed in most of these oxidases. The FAD-interacting residues seem more conserved on the adenine ringside than on the isoalloxazine ringside. The variation

of residues interacting with the isoalloxazine ringside appears to be significant in the evolution of FAD-dependent enzymes and their numerous functions, as these variations facilitate the accommodation of several substrates. These results are consistent with the earlier observation that LAOs do not cluster into well-defined groups[25].

Enzymatic activity

Li-rLAO showed no activity with most amino acid substrates, except for a low and reproducible activity with the amino acid substrate L-Arg. It is interesting to note that *Li*-rLAO was active up to 2 mM concentration of L-arginine. Above this concentration, enzyme activity was inhibited (data not shown).

Comparison of the active-site geometries of amino acid oxidases

Due to the absence or low activity of *Li*-rLAO with most of the L-amino acid substrates, the active site of *Li*-rLAO was examined and compared with those of the well-studied *C. rhodostoma* LAA (PDB id: 2IID) and *R. opacus* LAO (PDB id: 2JB2). Figure 4 *a* and *b* shows the residues that interact with FAD and those within 4 Å distance that could interact with the amino acid substrates in *C. rhodostoma* and *R. opacus* LAO respectively. The amino acid sequences of *C. rhodostoma*, *R. opacus* and *Li*-rLAO sequences were aligned, and equivalent residues likely to interact with substrates were identified (Supplementary Figure 2). In LAOs, a conserved arginine residue forms a hydrogen bond with the carboxyl group of the amino acid substrate. This residue is present in *R. opacus* and *C. rhodostoma* LAOs, but not in *Li*-rLAO. A comparison of the active site geometries showed that the structurally equivalent residue was glutamate in *Li*-rLAO (Figure 4 *c*) and glutamine in putrescine oxidase (Figure 4 *d*). The arginine in *R. opacus* and *C. rhodostoma* LAOs presumably is essential for the activity of amino acid oxidases. Therefore, it is not surprising that *Li*-rLAO is not active towards most amino acid substrates. The *Li*-rLAO active site exhibited greater structural similarity with amine oxidase than amino acid oxidases. Therefore, *Li*-rLAO was tested for activity with amine substrates. However, the enzyme did not show activity with any of the amines examined.

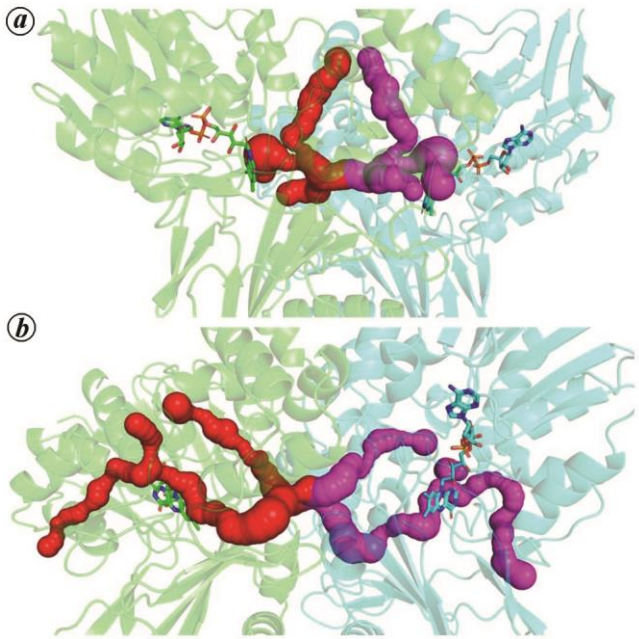

Figure 5. Identification of water-filled channels leading from bulk solvent to the active site of *Li*-rLAO using the CAVER tool. ***a***, Tunnels present in the interface of the crystal dimer of *Li*-rLAO. ***b***, Tunnels that lead to the active site of *Li*-rLAO.

Discussion

Catalysis by LAO requires three substrates – L-amino acid, molecular oxygen and a water molecule. The resulting products are an α-keto acid, hydrogen peroxide and an ammonium ion. The overall reaction of LAO has been described as two half-reactions[73]. In the first half of the reaction (also called the reductive half), FAD is reduced to $FADH_2$, leading to the oxidation of the bound amino acid to an imino acid[74,75]. The second half involves the oxidation of $FADH_2$, in which an oxygen molecule enters the active site of the enzyme, abstracts the hydrogen atoms from $FADH_2$ and gets converted to hydrogen peroxide, which exits from the active site. The different ways in which molecules enter and exit the active site during the reaction cycle have been studied. It has been suggested that lining of water molecules at the active site of LAO represent the entry–exit paths. It was possible to identify water-filled channels in *Li*-rLAO using the CAVER 3.03 program[76]. A tunnel in the interface is formed by chain A (residues Leu292– Leu298, Gly347, Asp348 and Pro402–Gly404) and chain B (residues Arg160–Asn165 and Asp190-Arg193; Figure 5 *a*); a second path constituted by peptide stretches Leu429–Leu437, Ile92–Ala99, Asn206–Tyr210, Ser320–Phe326, Asn181–Tyr187 and residues Ile103, Leu108, Lys109, Val214, Glu215, Leu221, Met218, Val299, Arg295, Arg349 and Ile398; another tunnel leading to FAD and limited by the peptide stretches Asn181–Ser191, Phe113–Val115, Ser320–Phe326 and Ile344–Arg349 and residues Tyr210 and Ile299, and a fourth path formed by the peptide stretches Gly347, Asp348, Tyr296–Arg298, Ala399–Phe401, Tyr187–Asp190 and Glu428–Asn430 and residues Leu195, Lys199 and Asp203 (Figure 5 *b*) could be identified. Despite the presence of these channels, *Li*-rLAO is not active with amino acid substrates, suggesting that the changes in residues close to the active site, in particular the absence of arginine conserved in other L-amino acid oxidases, are probably responsible for the lack of activity.

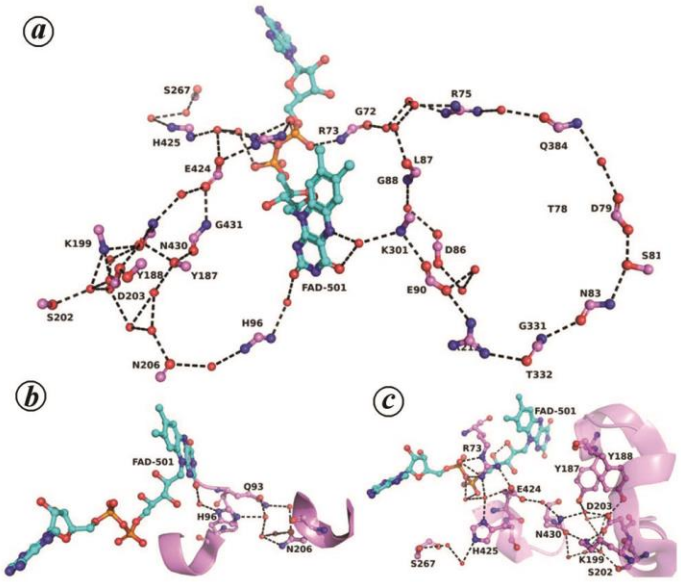

Figure 6. Structural analysis of *Li*-rLAO. ***a***, Hydrogen-bond networks observed in the *Li*-rLAO structure. ***b***, His95 forms a hydrogen bond network with C2 (C=O) of FAD. ***c***, His425 forms a hydrogen-bond network with the phosphate group of FAD.

Although *Li*-rLAO may catalyse a unique reaction distinct from the oxidation of amino acids, similarity in the structure of *Li*-rLAO and other amino acid oxidases suggests that it is worthwhile to consider the functional mechanism of LAOs. As mentioned earlier, in LAO, the reduction of FAD is proposed to follow one of the two mechanisms mentioned below. In the first mechanism, a proton is transferred to FAD from the Cα-atom of the substrate, leaving a negative charge on the carbon atom. This is followed by a two-electron transfer[77]. In the second mechanism, the Cα-hydrogen atom is transferred as a hydride ion carrying two electrons by a hydride transfer pathway[73]. In both these mechanisms, one hydrogen atom is added to each of the N1 and N5 atoms of the isoalloxazine ring. It has been proposed that there could be a direct translocation of proton/hydride ions to N5 of the isoalloxazine ring of FAD. With this background, it would be interesting to examine the plausible mechanism of a transfer of a proton/hydrogen atom from the substrate to the N1 atom of the isoalloxazine ring of FAD in LAOs. In Sv-LAO, His223 has been suggested to abstract the proton from the amino group of the substrate[78–80]. In the crystal structure of *C. rhodostoma* LAO, a short pathway that may be involved in the proton translocation has been observed from His223 to N1 of FAD. The residue structurally equivalent to His223 is not conserved in *Li*-rLAO. In spite of this change, two hydrogen-bond networks that link the substrate-binding residues to the oxygen atom of the C2 keto group of the isoalloxazine ring could be identified in *Li*-rLAO (Figure 6 *a*). The exciting aspect of these networks is that the water molecules positioned between polar side chains may facilitate proton translocation. These hydrogen-bond networks do not involve peptide backbone atoms, except for the peptide bond containing Gly residues. The flexibility due to the occurrence of glycine may facilitate the formation of this hydrogen bond network[81]. There are only two histidine residues in *Li*-rLAO. His96 forms a hydrogen bond with water, forming a hydrogen bond with the carbonyl of the second carbon atom of the FAD isoalloxazine ring (Figure 6 *b*). His425 forms a hydrogen-bond network with a water molecule, forming a hydrogen bond with the phosphate group of FAD (Figure 6 *c*). The significance of these histidine residues in *Li*-LAO is yet to be established. The absence of residues considered essential for the activity of *Li*-rLAO with amino acid substrates suggests that *Li*-rLAO may act on an unusual substrate. Further studies are needed for the identification of the reaction catalysed by *Li*-rLAO.

Conclusion

The putative *Li*-rLAO was cloned, expressed and purified to homogeneity and characterized by various biophysical methods. The structure of the recombinant protein was obtained by X-ray crystallography to a resolution of 1.8 Å. The polypeptide fold of *Li*-rLAO resembled that of the evolutionarily well-conserved FAD-binding amino acid oxidases. On the contrary, *Li*-rLAO lacked a conserved substrate-binding residue (arginine) compared with known LAO structures. *Li*-rLAO did not exhibit any activity with most of the L-amino acids, but had low activity only with L-arginine. *Li*-rLAO exhibited little or no activity with amines, including putrescine, spermine and spermidine. Further studies are needed to determine the specific biological role of *Li*-rLAO.

Conflict of interest: The authors declare that there is no conflict of interest.

1. Kobayashi, Y., Discovery of the causative organism of Weil's disease: historical view. *J. Infect. Chemother.*, 2001, **7**, 10–15.
2. Haake, D. A., Spirochaetal lipoproteins and pathogenesis. *Microbiology*, 2000, **146**(Pt 7), 1491–1504.
3. Cullen, P. A., Haake, D. A. and Adler, B., Outer membrane proteins of pathogenic spirochetes. *FEMS Microbiol. Rev.*, 2004, **28**, 291–318.
4. Trueba, G. A., Bolin, C. A. and Zuerner, R. L., Characterization of the periplasmic flagellum proteins of *Leptospira interrogans*. *J. Bacteriol*., 1992, **174**, 4761–4768.
5. Levett, P. N., Leptospirosis. *Clin. Microbiol. Rev.*, 2001, **14**, 296–326.
6. Adler, B. and de la Pena Moctezuma, A., Leptospira and leptospirosis. *Vet. Microbiol*., 2010, **140**, 287–296.
7. Marshall, R. B., The route of entry of leptospires into the kidney tubule. *J. Med. Microbiol*., 1976, **9**, 149–152.
8. Morrison, W. I. and Wright, N. G., Canine leptospirosis: an immunopathological study of interstitial nephritis due to *Leptospira canicola*. *J. Pathol*., 1976, **120**, 83–89.
9. Ballard, S. A., Williamson, M., Adler, B., Vinh, T. and Faine, S., Interactions of virulent and avirulent leptospires with primary cultures of renal epithelial cells. *J. Med. Microbiol.*, 1986, **21**, 59–67.
10. Yang, C. W., Wu, M. S. and Pan, M. J., *Leptospirosis* renal disease. *Nephrol. Dial. Transplant*., 2001, **16**(Suppl 5), 73–77.
11. Silbernagl, S., Kinetics and localization of tubular resorption of acidic amino-acids – a microperfusion and free-flow micropuncture study in rat-kidney. *Pflug. Arch. Eur. J. Physiol.*, 1983, **396**, 218–224.
12. Silbernagl, S. and Volkl, H., Molecular specificity of the tubular resorption of acidic amino-acids – a continuous microperfusion study in rat–kidney *in vivo*. *Pflug. Arch. Eur. J. Physiol.*, 1983, **396**, 225–230.
13. Brosnan, J. T., The 1986 Borden award lecture. The role of the kidney in amino acid metabolism and nutrition. *Can. J. Physiol. Pharmacol*., 1987, **65**, 2355–2362.
14. Silbernagl, S., The renal handling of amino acids and oligopeptides. *Physiol. Rev*., 1988, **68**, 911–1007.
15. Dantzler, W. H. and Silbernagl, S., Amino-acid transport by juxtamedullary nephrons – distal reabsorption and recycling. *Am. J. Physiol.*, 1988, **255**, F397–F407.
16. Nakanishi, T., Shimizu, A., Saiki, K., Fujiwara, F., Funahashi, S. and Hayashi, A., Quantitative analysis of urinary pyroglutamic acid in patients with hyperammonemia. *Clin. Chim. Acta*, 1991, **197**, 249–255.
17. van de Poll, M. C., Soeters, P. B., Deutz, N. E., Fearon, K. C. and Dejong, C. H., Renal metabolism of amino acids: its role in interorgan amino acid exchange. *Am. J. Clin. Nutr*., 2004, **79**, 185–197.
18. Hossain, G. S., Li, J. H., Shin, H. D., Du, G. C., Liu, L. and Chen, J., L-Amino acid oxidases from microbial sources: types, properties, functions, and applications. *Appl. Microbiol. Biotechnol*., 2014, **98**, 1507–1515.
19. Sacchi, S., Caldinelli, L., Cappelletti, P., Pollegioni, L. and Molla, G., Structure–function relationships in human D-amino acid oxidase. *Amino Acids*, 2012, **43**, 1833–1850.
20. Pollegioni, L., Sacchi, S. and Murtas, G., Human D-amino acid oxidase: structure, function, and regulation. *Front. Mol. Biosci*., 2018, **5**, 107.
21. Hughes, A. L., Origin and diversification of the L-amino oxidase family in innate immune defenses of animals. *Immunogenetics*, 2010, **62**, 753–759.
22. Kasai, K., Ishikawa, T., Nakamura, T. and Miura, T., Antibacterial properties of L-amino acid oxidase: mechanisms of action and perspectives for therapeutic applications. *Appl. Microbiol. Biotechnol*., 2015, **99**, 7847–7857.
23. Du, X. Y. and Clemetson, K. J., Snake venom L-amino acid oxidases. *Toxicon*, 2002, **40**, 659–665.
24. Izidoro, L. F. *et al.*, Snake venom L-amino acid oxidases: trends in pharmacology and biochemistry. *Biomed Res Int*., 2014, **2014**, 196754.
25. Campillo-Brocal, J. C., Lucas-Elio, P. and Sanchez-Amat, A., Distribution in different organisms of amino acid oxidases with FAD or a quinone as cofactor and their role as antimicrobial proteins in marine bacteria. *Mar. Drugs*, 2015, **13**, 7403–7418.
26. Pawelek, P. D., Cheah, J., Coulombe, R., Macheroux, P., Ghisla, S. and Vrielink, A., The structure of L-amino acid oxidase reveals the substrate trajectory into an enantiomerically conserved active site. *EMBO J.*, 2000, **19**, 4204–4215.
27. Leese, C., Fotheringham, I., Escalettes, F., Speight, R. and Grogan, G., Cloning, expression, characterization and mutational analysis of L-aspartate oxidase from *Pseudomonas putida*. *J. Mol. Catal. B-Enzym.*, 2013, **85–86**, 17–22.
28. Liu, L., Hossain, G. S., Shin, H. D., Li, J., Du, G. and Chen, J., One-step production of alpha- ketoglutaric acid from glutamic acid with an engineered L-amino acid deaminase from *Proteus mirabilis*. *J. Biotechnol*., 2013, **164**, 97–104.
29. Geueke, B. and Hummel, W., A new bacterial L-amino acid oxidase with a broad substrate specificity: purification and characterization. *Enzyme Microb. Technol.*, 2002, **31**, 77–87.
30. Eshghi, A., Pappalardo, E., Hester, S., Thomas, B., Pretre, G. and Picardeau, M., Pathogenic *Leptospira interrogans* exoproteins are primarily involved in heterotrophic processes. *Infect. Immunol*., 2015, **83**, 3061–3073.
31. Fouts, D. E. *et al.*, What makes a bacterial species pathogenic? Comparative genomic analysis of the genus *Leptospira*. *PLoS Negl. Trop. Dis*., 2016, **10**, e0004403.
32. Altschul, S. F., Madden, T. L., Schaffer, A. A., Zhang, J., Zhang, Z., Miller, W. and Lipman, D. J., Gapped BLAST and PSI-BLAST: a new generation of protein database search programs. *Nucleic Acids Res*., 1997, **25**, 3389–3402.
33. Finn, R. D. *et al.*, Pfam: the protein families database. *Nucleic Acids Res*., 2014, **42**, D222–D230.
34. Marchler-Bauer, A. *et al.*, CDD: NCBI's conserved domain database. *Nucleic Acids Res*., 2015, **43**, D222–D226.
35. Boratyn, G. M. *et al.*, BLAST: a more efficient report with usability improvements. *Nucleic Acids Res.*, 2013, **41**, W29–W33.
36. Shevchenko, A., Tomas, H., Havlis, J., Olsen, J. V. and Mann, M., In-gel digestion for mass spectrometric characterization of proteins and proteomes. *Nature Protoc.*, 2006, **1**, 2856–2860.
37. Winn, M. D. *et al.*, Overview of the CCP4 suite and current developments. *Acta Crystallogr. D, Biol. Crystallogr*., 2011, **67**, 235–242.
38. Winter, G., xia2: An expert system for macromolecular crystallography data reduction. *J. Appl. Crystallogr*., 2010, **43**, 186–190.
39. Winter, G. *et al.*, DIALS: implementation and evaluation of a new integration package. *Acta Crystallogr. D, Struct. Biol*., 2018, **74**, 85–97.
40. Evans, P., Scaling and assessment of data quality. *Acta Crystallogr. D, Biol. Crystallogr*., 2006, **62**, 72–82.
41. Evans, P. R. and Murshudov, G. N., How good are my data and what is the resolution? *Acta Crystallogr. D, Biol. Crystallogr.*, 2013, **69**, 1204–1214.
42. Evans, P. R., An introduction to data reduction: space-group determination, scaling and intensity statistics. *Acta Crystallogr. D, Biol. Crystallogr.*, 2011, **67**, 282–292.
43. Panjikar, S., Parthasarathy, V., Lamzin, V. S., Weiss, M. S. and Tucker, P. A., Auto-rickshaw: an automated crystal structure determination platform as an efficient tool for the validation of an X-ray diffraction experiment. *Acta Crystallogr. D, Biol. Crystallogr*., 2005, **61**, 449–457.
44. Panjikar, S., Parthasarathy, V., Lamzin, V. S., Weiss, M. S. and Tucker, P. A., On the combination of molecular replacement and single-wavelength anomalous diffraction phasing for automated

structure determination. *Acta Crystallogr. D, Biol. Crystallogr*., 2009, **65**, 1089–1097.
45. Hatti, K., Biswas, A., Chaudhary, S., Dadireddy, V., Sekar, K., Srinivasan, N. and Murthy, M. R. N., Structure determination of contaminant proteins using the MarathonMR procedure. *J. Struct. Biol*., 2017, **197**, 372–378.
46. Skubak, P. and Pannu, N. S., Automatic protein structure solution from weak X-ray data. *Natrue Commun*., 2013, **4**, 2777.
47. Sheldrick, G. M., A short history of SHELX. *Acta Crystallogr. A*, 2008, **64**, 112–122.
48. Schneider, T. R. and Sheldrick, G. M., Substructure solution with SHELXD. *Acta Crystallogr. D, Biol. Crystallogr*., 2002, **58**, 1772–1779.
49. Murshudov, G. N. *et al.*, REFMAC5 for the refinement of macromolecular crystal structures. *Acta Crystallogr. D, Biol. Crystallogr*., 2011, **67**, 355–367.
50. Abrahams, J. P. and Leslie, A. G., Methods used in the structure determination of bovine mitochondrial F1 ATPase. *Acta Crystallogr. D, Biol. Crystallogr*., 1996, **52**, 30–42.
51. Skubak, P., Waterreus, W. J. and Pannu, N. S., Multivariate phase combination improves automated crystallographic model building. *Acta Crystallogr. D, Biol. Crystallogr*., 2010, **66**, 783–788.
52. Cowtan, K., Recent developments in classical density modification. *Acta Crystallogr. D, Biol. Crystallogr*., 2010, **66**, 470–478.
53. Cowtan, K., The Buccaneer software for automated model building. 1. Tracing protein chains. *Acta Crystallogr. D, Biol. Crystallogr*., 2006, **62**, 1002–1011.
54. Emsley, P., Lohkamp, B., Scott, W. G. and Cowtan, K., Features and development of Coot. *Acta Crystallogr. D, Biol. Crystallogr*., 2010, **66**, 486–501.
55. Kovalevskiy, O., Nicholls, R. A., Long, F., Carlon, A. and Murshudov, G. N., Overview of refinement procedures within REFMAC5: utilizing data from different sources. *Acta Crystallogr. D, Struct. Biol*., 2018, **74**, 215–227.
56. Murshudov, G. N., Vagin, A. A. and Dodson, E. J., Refinement of macromolecular structures by the maximum-likelihood method. *Acta Crystallogr. D, Biol. Crystallogr*., 1997, **53**, 240–255.
57. Murshudov, G. N., Vagin, A. A., Lebedev, A., Wilson, K. S. and Dodson, E. J., Efficient anisotropic refinement of macromolecular structures using FFT. *Acta Crystallogr. D, Biol. Crystallogr*., 1999, **55**, 247–255.
58. Nicholls, R. A., Long, F. and Murshudov, G. N., Low-resolution refinement tools in REFMAC5. *Acta Crystallogr. D, Biol. Crystallogr*., 2012, **68**, 404–417.
59. Vagin, A. A., Steiner, R. A., Lebedev, A. A., Potterton, L., McNicholas, S., Long, F. and Murshudov, G. N., REFMAC5 dictionary: organization of prior chemical knowledge and guidelines for its use. *Acta Crystallogr. D, Biol. Crystallogr.*, 2004, **60**, 2184–2195.
60. Winn, M. D., Murshudov, G. N. and Papiz, M. Z., Macromolecular TLS refinement in REFMAC at moderate resolutions. *Methods Enzymol.*, 2003, **374**, 300–321.
61. Vagin, A. and Teplyakov, A., Molecular replacement with MOLREP. *Acta Crystallogr. D, Biol. Crystallogr.*, 2010, **66**, 22–25.
62. Lebedev, A. A., Vagin, A. A. and Murshudov, G. N., Model preparation in MOLREP and examples of model improvement using X-ray data. *Acta Crystallogr. D, Biol. Crystallogr*., 2008, **64**, 33–39.
63. Krissinel, E. and Henrick, K., Inference of macromolecular assemblies from crystalline state. *J. Mol. Biol*., 2007, **372**, 774–797.
64. Krissinel, E., Crystal contacts as nature's docking solutions. *J. Comput. Chem*., 2010, **31**, 133–143.
65. Krissinel, E., Enhanced fold recognition using efficient short fragment clustering. *J. Mol. Biochem.*, 2012, **1**, 76–85.
66. Holm, L. and Sander, C., Dali: a network tool for protein structure comparison. *Trends Biochem. Sci*., 1995, **20**, 478–480.
67. Holm, L. and Sander, C., Mapping the protein universe. *Science*, 1996, **273**, 595–603.
68. Holm, L., DALI and the persistence of protein shape. *Protein Sci*., 2020, **29**, 128–140.
69. Hasegawa, H. and Holm, L., Advances and pitfalls of protein structural alignment. *Curr. Opin. Struct. Biol*., 2009, **19**, 341–348.
70. Kishimoto, M. and Takahashi, T., A spectrophotometric microplate assay for L-amino acid oxidase. *Anal. Biochem*., 2001, **298**, 136–139.
71. Holt, A. and Palcic, M. M., A peroxidase-coupled continuous absorbance plate-reader assay for flavin monoamine oxidases, copper-containing amine oxidases and related enzymes. *Nature Protoc*., 2006, **1**, 2498–2505.
72. Schwinn, K., Ferre, N. and Huix-Rotllant, M., UV–visible absorption spectrum of FAD and its reduced forms embedded in a cryptochrome protein. *Phys. Chem. Chem. Phys*., 2020, **22**, 12447–12455.
73. Fitzpatrick, P. F., Carbanion versus hydride transfer mechanisms in flavoprotein-catalyzed dehydrogenations. *Bioorg. Chem*., 2004, **32**, 125–139.
74. Mathews, F. S., New flavoenzymes. *Curr. Opin. Struc. Biol*., 1991, **1**, 954–967.
75. Dym, O. and Eisenberg, D., Sequence–structure analysis of FAD-containing proteins. *Protein Sci*., 2001, **10**, 1712–1728.
76. Stourac, J. *et al.*, Caver Web 1.0: identification of tunnels and channels in proteins and analysis of ligand transport. *Nucleic Acids Res.*, 2019, **47**, W414–W422.
77. Faust, A., Niefind, K., Hummel, W. and Schomburg, D., The structure of a bacterial L-amino acid oxidase from *Rhodococcus opacus* gives new evidence for the hydride mechanism for dehydrogenation. *J. Mol. Biol*., 2007, **367**, 234–248.
78. Georgieva, D., Murakami, M., Perband, M., Arni, R. and Betzel, C., The structure of a native L-amino acid oxidase, the major component of the *Vipera ammodytes ammodytes* venomic, reveals dynamic active site and quaternary structure stabilization by divalent ions. *Mol. Biosyst.*, 2011, **7**, 379–384.
79. Moustafa, I. M., Foster, S., Lyubimov, A. Y. and Vrielink, A., Crystal structure of LAAO from *Calloselasma rhodostoma* with an L-phenylalanine substrate: insights into structure and mechanism. *J. Mol. Biol*., 2006, **364**, 991–1002.
80. Ullah, A., Structure–function studies and mechanism of action of snake venom L-amino acid oxidases. *Front Pharmacol.*, 2020, **11**, 110.
81. Ramasarma, T. and Vaigundan, D., Pathways of electron transfer and proton translocation in the action of superoxide dismutase dimer. *Biochem. Biophys. Res. Commun*., 2019, **514**, 772–776.

ACKNOWLEDGEMENTS. We thank MBU, IISc, for permission to use its facilities and Elettra Synchrotron Trieste, Italy for data collection. We also thank Prof. P. Balaram (MBU, IISc) for his invaluable guidance during this study. D.V. thanks Prof. B. Gopal (MBU, IISc) for timely support and financial assistance and Profs. S. Ramkumar, A. Pennmetsa, J. Chatterjee, R. Varadarajan, S. Sharma, A. Surolia, M. Vijayan, R. Roy, D. N. Rao, Dr M. Vijaya Parthasarathy and Ms Debashree Behera from IISc, Bengaluru; Prof. H. Balaram (MBGU, JNCASR), Prof. M. K. Mathew, Dr Sanjeev Kumar (NCBS) and Dr H. T. Srinivasa, RRI, Bengaluru for their support and generous gift of chemicals. This article is dedicated to the memory of Prof. T. Ramasarma (deceased 22 February 2020), who has inspired a generation of protein chemists. This study was partially supported by Sri Devaraj Urs Academy of Higher Education and Research, Kolar (Grant ID: SDUAHER/Res.Proj/67/2013-14).

Received 1 February 2022; revised accepted 25 July 2022

doi: 10.18520/cs/v123/i7/895-906